Droplet detachment behavior from a rough hydrophilic surface

C. T. Wang[1], W. T. Leung[1], J. C. Xu[1], S. C. Fu[2], and Christopher Y. H. Chao[2]*

[1] Department of Mechanical and Aerospace Engineering, The Hong Kong University of Science and Technology, Hong Kong, China

[2] Department of Mechanical Engineering, The University of Hong Kong, Hong Kong, China

[*]Corresponding author: *cyhchao@hku.hk*

Address all correspondence to:

Christopher Y. H. Chao

Dean of Engineering and Chair Professor of Mechanical Engineering

The University of Hong Kong

Pokfulam,

Hong Kong, China

Email: cyhchao@hku.hk

Fax: (852) 2858-5415

Tel: (852) 3917-2800

ABSTRACT:

Understanding of the droplet detachment behavior from rough hydrophilic surfaces is important in many biological and industrial applications such as biomedicine, surface coating, and pathogen-laden aerosol resuspension. Due to the partial detachment of the droplet on hydrophilic surfaces, leaving behind some droplet residues, the adhesion behavior is extremely complicated. Here we reveal a new adhesion mechanism between a droplet and a rough hydrophilic surface. The adhesion behavior is controlled by a liquid film stuck in the surface microstructure. We establish a model to describe the contributions of liquid film and naked solid peaks, to the work of adhesion and verify the model experimentally. We also find that the normal adhesion force is about 3.35±0.25 times of the lateral adhesion force for different surface roughness, meaning that the separation direction is an important factor affecting adhesion due to the different separation mechanisms. The results of this work shed new insights on the understanding of droplet detachment and adhesion to a rough surface.

Keywords: Work of adhesion; Microdroplet; Surface roughness; Detachment behavior; Liquid film

1. Introduction

Understanding of the droplet detachment from rough hydrophilic surfaces is of great importance in a variety of applications and phenomena, including hydrophilic coatings of biomaterials (Kanematsu and Yoshitake 2015, Wyman 2012) , lipase immobilized on a hydrophilic membrane (Giorno et al. 2003), and resuspension of pathogen-laden saliva droplet from indoor surfaces

(Prussin and Marr 2015). Both the migration of deposited microdroplets to other surfaces and resuspension due to air flow or human activities can be a new infectious pathogen source to building environment and pose potential threat to human health (Lei et al. 2017, Leung et al. 2017, Rheinbaben et al. 2000, Rusin et al. 2002). In these processes, the adhesion between droplet and solid surface is the key parameter determining whether the droplet detachment happens. Although some researchers have studied the droplet detachment behaviour from smooth surfaces (Fu et al. 2018, Leung et al. 2013), the surfaces in building and industry environments are normally rough and hydrophilic, which changes the contact properties between droplet and surface and complicates the aerosol detachment behaviour (Quéré 2008, Wenzel 1949).

In order to study the detachment behaviour and adhesion of a droplet on a rough surface, extensive researches have been conducted by fabricating the surfaces using micro-textures or micro-pillars (Jiang et al. 2017, Miwa et al. 2000, Paxson and Varanasi 2013, Xu and Choi 2012, Yoshimitsu et al. 2002). In general, when a droplet sits on a rough hydrophobic surface, its three-phase contact line is pinned on the micropillars (Xu and Choi 2012). The droplet can be in Wenzel state in which the liquid sticks and fills in the asperities (Wenzel 1936, Wenzel 1949), or Cassie state that air is trapped in between the asperities (Cassie and Baxter 1944), depending on the pillar dimensions (Boreyko and Chen 2009, He et al. 2003, Koishi et al. 2009, Lafuma and Quéré 2003). Although the hydrophobicity of a hydrophobic solid surface is always enhanced by roughness, the work of adhesion increases or decreases depending on whether the droplet is in Wenzel state or Cassie state respectively. On the other hand, for the droplet on a rough hydrophilic surface, the liquid can penetrate the surface structures resulting in the Wenzel state. Introduction of roughness makes the surface more hydrophilic. Moreover, the contact line is much more strongly pinned by

3

the peaks and troughs of surface features, so that the droplet may split into portions during the detachment process (Fu et al. 2014, Fu et al. 2018, Leung et al. 2013). Since Young-Dupré equation assumes that the separation of the droplet from the solid leaving behind a clean solid surface, due to the partial detachment of the droplet on hydrophilic surfaces, the liquid film or smaller droplet leaving behind causes a difficulty in applying Young-Dupré equation to determine the work of adhesion. Despite the fact that the droplet detachment behaviour from a solid smooth surface has been understood to a certain extent, the study of the detachment behaviour and adhesion of a droplet to a rough hydrophilic surface are still lacking.

In this research, we focus on figuring out how the surface roughness affects the detachment behaviour and adhesion of a droplet to a rough hydrophilic surface, and how the applied force direction affects the adhesion. An ultracentrifuge was employed to provide normal and lateral force to the droplets. Hydrophilic substrates with different roughness were fabricated. After the droplet separation from the rough hydrophilic surface, the adhesion was determined, and a liquid film was found leaving on the surface. The relationship between the adhesion and the liquid film was also examined.

2. Experimental materials and method

In this study, glycerol-water solution was used to prepare the microdroplets because it can retain a specific glycerol weight ratio under a specific temperature and humidity (Flick 1998). Furthermore, it has been used to simulate the nonvolatile organic or protein component in many pesticide or salivary excretion studies (Bergeron et al. 2000, Fu et al. 2018, Leung et al. 2013). The microdroplets were generated by a Vibrating Orifice Aerosol Generator (VOAG) and then

deposited on poly (methyl methacrylate) (PMMA) substrates with different contact diameters of about 100-200 μm. The samples were put in a chamber at a controlled temperature of 20 ℃, and relative humidity of 70% for 12 hours, under which the glycerol weight ratio increased from initial ratio 25% to equilibrium ratio 64.68% by water evaporation. At this percentage, the density of the glycerol-water mixture was measured to be 1126.9 kg/m^3 (Flick 1998).

PMMA substrates with 6 different roughness were fabricated from commercial smooth PMMA by a grinder polisher machine. The Young's Modulus of PMMA is around 3 GPa and the strength is around 70 MPa. In the experiment, the pressure acting on the substrate from the centrifugal force was around 10^{-3} Pa, which was much smaller than the strength of PMMA. There was no sample fracture or deformation observed in the experiment. The substrate size was 12×12×2 mm (L× W× H). The solid substrates were not reused due to the residue of glycerol-water liquid and possible damage from the high centrifugal force. Roughness, Ra, of the rough samples was measured by an optical profiler (NPFLEX, Bruker Nano, Inc., USA). The roughness of the smooth surface, commercially available smooth PMMA without abrasion, was measured by an atomic force microscope (AFM, NanoScope IIIa/Dimension 3100, Veeco Instruments Inc., USA) due to the nanoscale roughness. The rough surface structures were randomly but uniformly distributed because the roughness at x and y directions were almost identical. Contact angle, θ, of the droplets on the surfaces were measured by a goniometer (Biolin Theta Contact Angle Meter C204A, Biolin Scientific, Sweden). Surface tension of the droplet in equilibrium was measured as 64.8 ± 0.4 mN/m by a goniometer based on the pendant drop (Adamson and Gast 1967). The contact diameter of a droplet, D, was captured by a camera connected with a microscope. The contact angles were less than 90º, so the observed droplet edge was the real contact line.

In this work, ultracentrifuge (CP80WX, Hitachi, Japan) was employed to provide both normal and lateral removal forces. Substrates were fixed in customized holders that were put into normal or lateral directions for centrifuge. Distance between the sample and axis of rotation, R, was 0.074 m. The schematic diagram of the experimental setup is shown in Fig. 1.
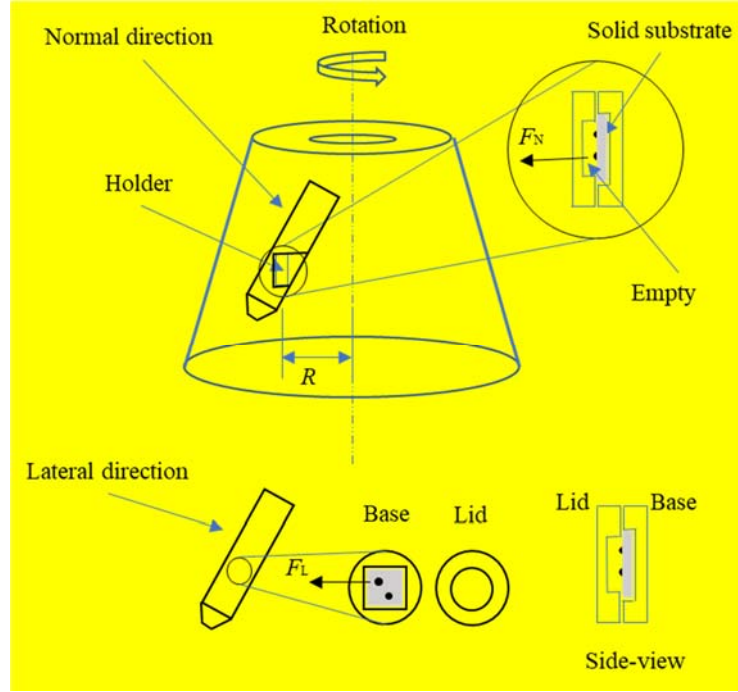

Fig. 1. Schematic diagram of the experimental setup for normal and lateral direction cases

The gravitational force on the microdroplets (10^{-9} - 10^{-8} N, Diameter: 100-200 μm) was negligible compared with the centrifugal force in the experiment (10^{-5} N). In the rotational process, the holder was enclosed, and so there was no air movement inside the holder, thus no aerodynamic force was applied to the droplets. The centrifugal force under a specific rotational speed, ω, was calculated by the following equation:

$$F = \rho V \omega^2 R \qquad (1)$$

The initial droplet volume, V, was calculated by the following spherical cap equation (Fu et al. 2018, Leung et al. 2013, Tadmor 2004) due to the rather small Bond number at the static status ($Bo = \rho g h^2 / \gamma_{\mathrm{L}} = 10^{-4}$, h: droplet height, γ_{L}: liquid surface tension), which indicates that surface tension dominates in microdroplets.

$$V = \frac{\pi}{24} \frac{(1-cos\theta)(sin^2\theta + 1 - cos\theta)}{sin^3\theta} D^3 \qquad (2)$$

where θ is the apparent contact angle, and D is the contact diameter of a microdroplet on a surface.

2.1. Normal adhesion force per unit length

The following equation was used to get the normal adhesion force per unit length, W_{N} , (Gulec et al. 2017, Tadmor et al. 2017):

$$W_{\mathrm{N}} = \frac{F_{\mathrm{N}}}{\pi D_{\mathrm{c}}} \qquad (3)$$

where F_{N} and D_{C} are the normal force and the contact diameter at the critical point, where the droplet can spontaneously recede from the surface without further increasing of the normal force and partially detaches by necking and rupturing, leaving behind a smaller droplet. The value of W_{N} can also represent the work of adhesion (WA) (Tadmor et al. 2017) which is the energy difference of the droplet-surface system per unit contact area before and after the droplet detachment (Dupré and Dupré 1869).

In this work, the critical contact diameter of the droplet cannot be directly captured by mounting a camera in the ultracentrifuge due to the limited space in the centrifuge and high rotational speed (8,000-20,000 RPM). Therefore, instead of continuously monitoring the droplet, we increased the rotational speed stepwise from 0 RPM until the droplet detached. Each time, we took a picture under a microscope, and measured the contact diameter of each droplet. Then we increased the

speed by 500 RPM or 1,000 RPM. After rotation, we took a picture under a microscope again and repeated the procedure. When the rotational speed was increased from ω_A to ω_B, the droplet contact diameter reduced from D_1, to a smaller value, D_2, of the remaining droplet due to partial detachment. The corresponding normal forces F_A and F_B were calculated by Eq. (1) with contact diameter D_1. Since in the droplet separation process, the critical diameter, D_C, was between D_1, and D_2, in calculating W_N, D_C was approximated by the mean of D_1 and D_2, while F_N was approximated by the mean of F_A and F_B. The uncertainty of W_N was measured from the differences, $(D_2 - D_1)$ and $(F_B - F_A)$.The detachment process is illustrated in Fig. 2.
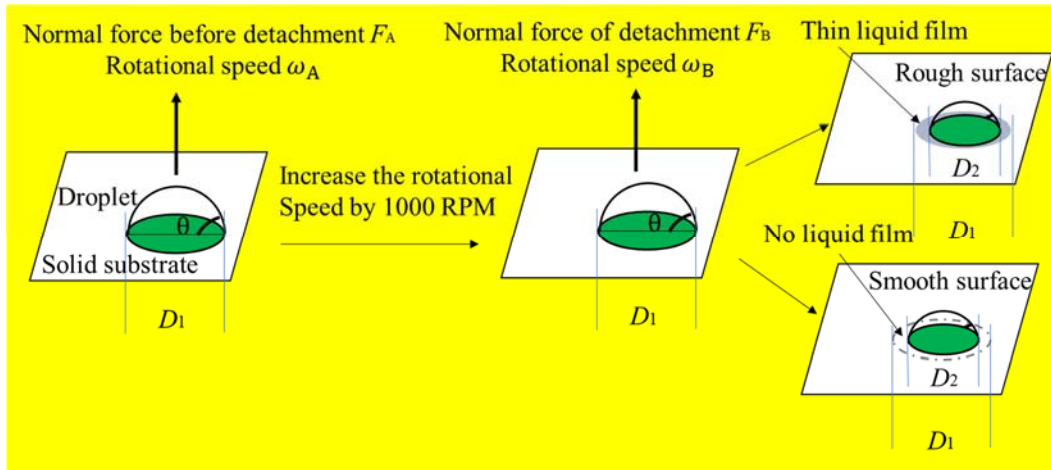
Fig. 2. Schematic diagram of droplet detachment under normal force. F_A and F_B are the normal centrifugal forces just before and after detachment. After normal detachment, a smaller droplet is left surrounded by a thin liquid film for the rough surfaces. There is no liquid film surrounding the remaining droplet on the smooth surface.

2.2. Lateral adhesion force per unit length

8

The following equation was used to calculate the lateral adhesion force per unit length, W_L, which is based on the fact that the ratio of retention force to droplet contact radius/diameter is a constant for specific droplet-surface system (Dussan 1985, Extrand and Gent 1990):

$$W_L = \frac{F_L}{\pi D_c} \qquad (4)$$

where F_L and D_c are the critical lateral force, and the contact diameter at the critical point, where the droplet starts the detachment, respectively.

For both millimeter droplets and microdroplets, the droplets slide from the solid substrate when the lateral force exceeds a critical value (Fu et al. 2018, Tadmor et al. 2017) . In order to get the critical lateral force, F_L, the rotational speed was also increased gradually from 0 RPM until the droplet slides. When the rotational speed was increased from ω_A to ω_B, the droplet detached totally from the surface, and the corresponding lateral forces F_A and F_B were calculated by Eq. (1) with contact diameter D_I. In estimating W_L, the critical lateral force was approximated by the mean value of F_A and F_B and the critical contact diameter, D_c, was equal to D_I. The uncertainty of W_L was measured from the difference of the two lateral forces, F_A and F_B. The droplet detachment process is illustrated in Fig. 3.
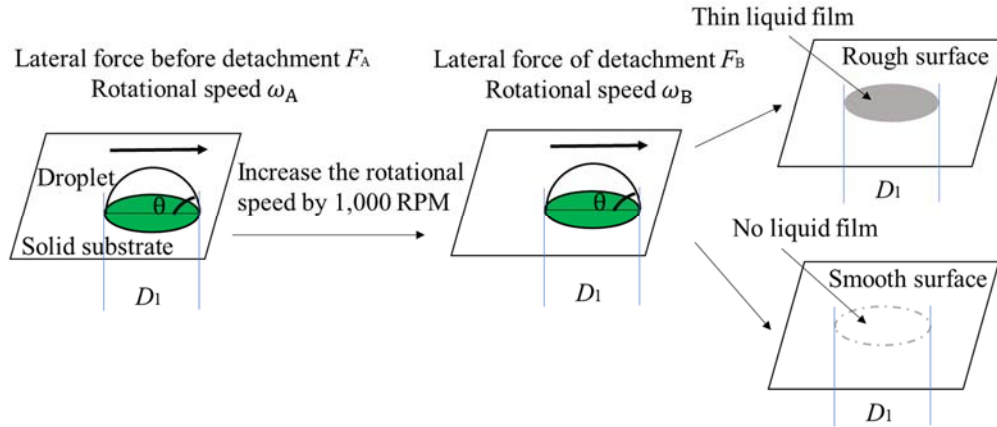
Fig. 3. Schematic diagram of droplet detachment under lateral force. F_A and F_B are the lateral centrifugal forces just before and after detachment. After detachment, a droplet on a rough surface leaves behind a liquid film, but a droplet on a smooth surface does not leave behind a liquid film at the original place.

3. Results

Samples with six different surface roughness from 0.0011 μm to 1.53 μm were prepared and investigated. It was observed that for both force directions, a droplet did not detach from the surface until the force reached a critical value. A droplet under normal force detached partially, leaving behind a smaller droplet, but under lateral force, it detached totally without leaving behind a smaller droplet, or leaving behind a negligible small amount of droplet. When the applied force is a little lower than the critical value, the droplet contact line may change slightly, especially on the case of rough surface under lateral force. This was also reported to be observed in the case of a rather large droplet (1-2 mm in diameter) on a smooth PMMA surface under the shear force of an approaching wind in a wind tunnel (Fu et al. 2014). It means that the depinning force on the contact line is not uniform in some cases and the local contact line can shrink a little before droplet

10

detachment. Fig. 4 shows the pictures under a microscope illustrating the detachment of droplets under normal and lateral forces. By comparing Fig. 4a and 4c, we can see that under the same force field, the left droplet on rough surface is much larger than that on smooth surface. It means the rough surface has much larger adhesion force to liquid droplet than smooth surface, which is different from the phenomenon that rough surface has smaller adhesion force to solid particle (Hontanon et al. 2000). Based on force balance model for particle resuspension in turbulent flows, they found that the adhesion force between solid particle and rough surface decreases as the increases of surface roughness and is much less than that for smooth surface.
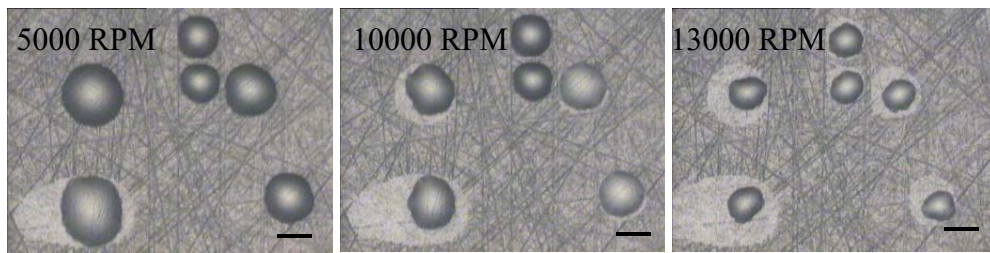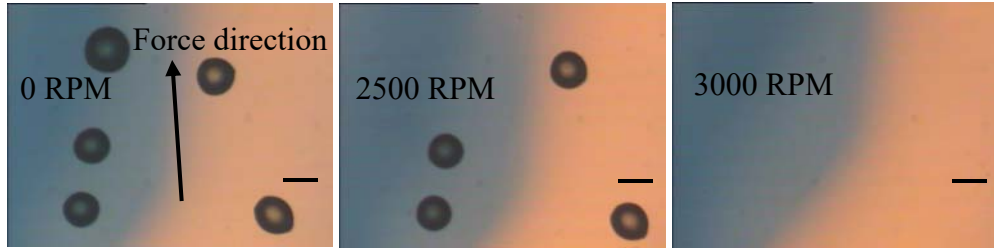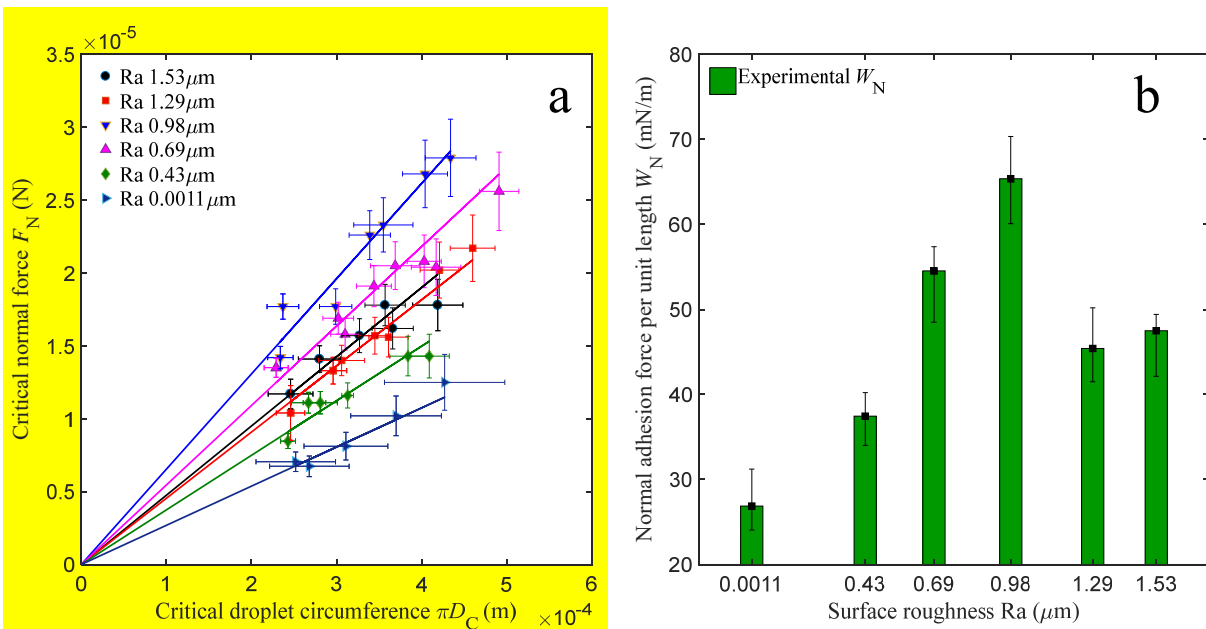

(a) Normal force
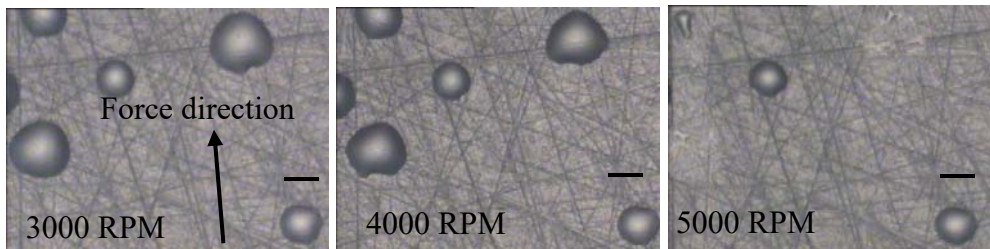
(b) Lateral force

(c) Normal force

(d) Lateral force

Detachment of droplets under normal force and lateral force on (a) and (b), a rough surface (Ra=0.69 µm); (c) and (d), a smooth surface (Ra=0.0011µm). The scale bars are all 100 µm.

The plots of adhesion force against droplet circumference with different surface roughness are shown in Fig. 5, and linear relations were found. According to equation (3), the slopes of the linear lines represent the W_N and W_L. It clearly shows that the work of adhesion (W_N) of microdroplets is independent of droplet size and is a surface-droplet system property for each roughness.
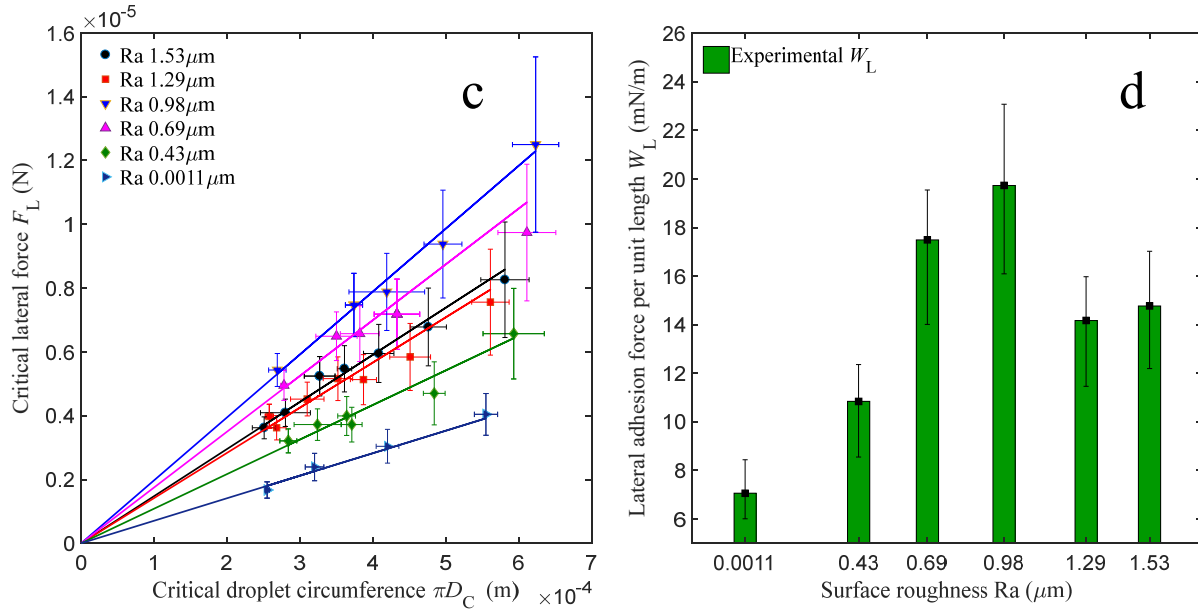
Fig. 5. Plots of (a) and (b) critical normal force, and (c) and (d) critical lateral force against critical droplet circumference. The vertical and horizontal error bars in (a) are the differences of the forces and circumferences before and after detachment, respectively; the vertical and horizontal error bars in (c) are the two successively applied lateral forces and the standard deviation of detached microdroplet sizes, respectively. The vertical error bars in (b) and (d) are the adhesion ranges.

The work of adhesion, W_N from the experiments for each roughness is plotted in Fig. 5b. As the surface roughness increases, the W_N first increases almost linearly and reaches the largest value at about 65 mN/m with roughness of 0.98 μm, beyond which the W_N decreases rapidly and almost remains constant even though the Ra is further increased. The W_L shows the same trend with surface roughness: linear increase stage, rapid drop stage, and basin stage, as shown in Fig. 5d. The largest W_L also happens at roughness 0.98 μm.

4. Discussion

4.1. Normal adhesion force per unit length, W_N, of droplets to a rough hydrophilic surface

As shown in Fig. 6, liquid films were left on the rough surfaces and surrounded the remaining droplets after the droplet separation process.
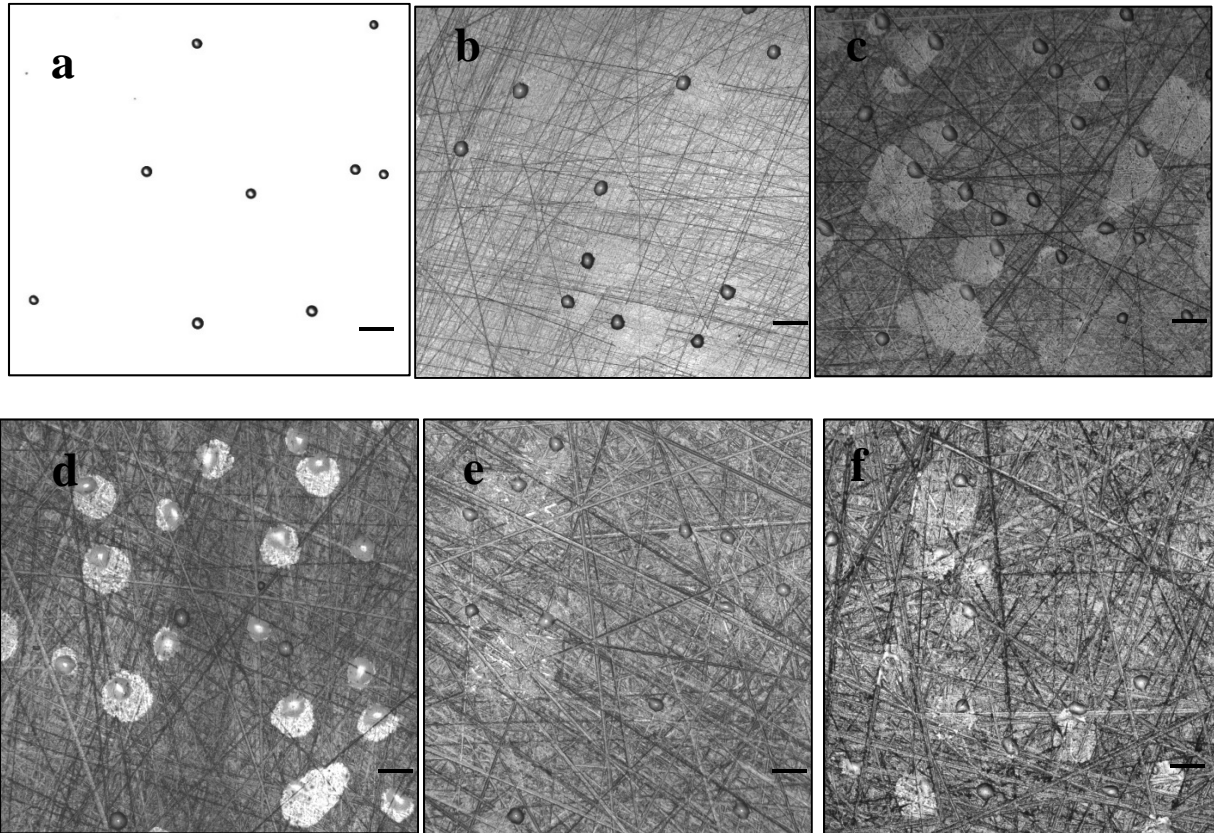

Fig. 6. Liquid films around the microdroplets after partial detachment under normal force. The rotational speed was increased stepwise for a number of times up to 20,000 RPM in order to detach more liquid and show larger area of liquid film for illustrative purpose. (a)-(f) are the surfaces with roughness: 0.0011, 0.43, 0.69, 0.98, 1.29, and 1.53 μm, respectively. The scale bars are 150 μm.

It is believed that during the detachment process, the droplet three-phase contact line shrinks on the rough surface and the liquid inside the surface microstructures partially or fully detached, forming the remaining liquid film. It indicates that the droplet detachment process consists of both liquid-liquid separation and liquid-solid separation. Thus, the overall work of adhesion W_N is proposed as a linear combination of liquid-liquid adhesion and solid-liquid adhesion:

$$W_N = f \cdot \gamma_L + (1 - f) \cdot r \cdot W_{S,L} \tag{6}$$

where f is the ratio of the liquid-liquid contact line projection length to the overall contact line projection length at the critical point of detachment defining in Fig. 7 and Equation (7), γ_L is the liquid surface tension , r, length density, is the ratio of actual surface profile length to the projection length of the rough surface, based on the surface profile measured from an optical profiler, and $W_{S,L}$ is the work of adhesion of a smooth surface. In this work, $W_{S,L}$ is obtained by the case of Ra=0.0011μm which is two orders smaller in magnitude than that of the studied rough surfaces. The first term on the right-hand side of Equation (6) represents the liquid-liquid separation and the second term represents the liquid-solid separation. The calculation schematic and measured results of the length density are shown in Figure 1S, Figure 2S, and Table 1S in the Supporting Information.
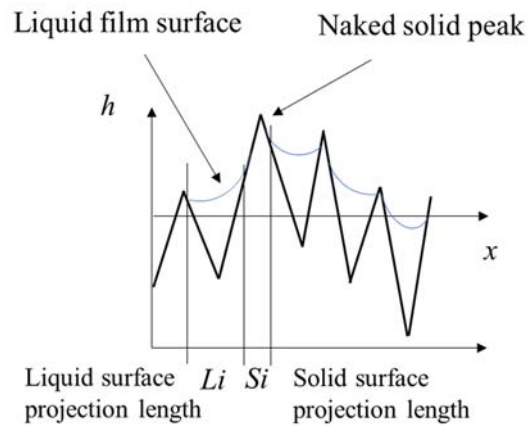

15

Fig. 7. The schematic diagram of effective remaining liquid and solid surface area
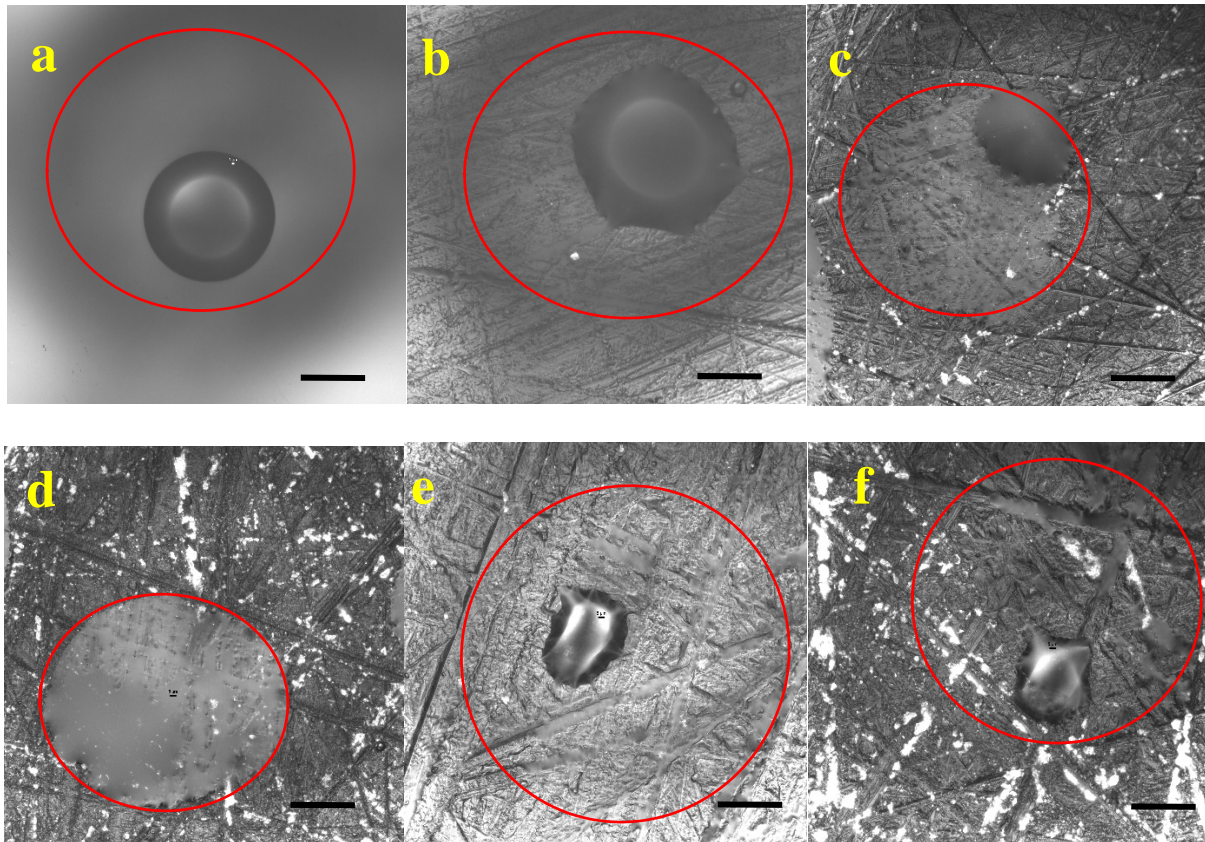
$$f = \frac{\sum Li}{\sum Li + \sum Si} \qquad (7)$$

Fig. 8. Liquid films after normal droplet detachment. The rotational speed is increased stepwise for a number of times up to 20,000 RPM in order to detach more liquid and show larger area of liquid film for illustrative purpose. Red circles indicate the original positions of the droplets before detachment. (a)-(f) are the surfaces with roughness: 0.0011, 0.43, 0.69, 0.98, 1.29, and 1.53 μm, respectively. Scale bars in (a) and (b) are 25 μm; the scale bars in (c)-(f) are 50 μm.
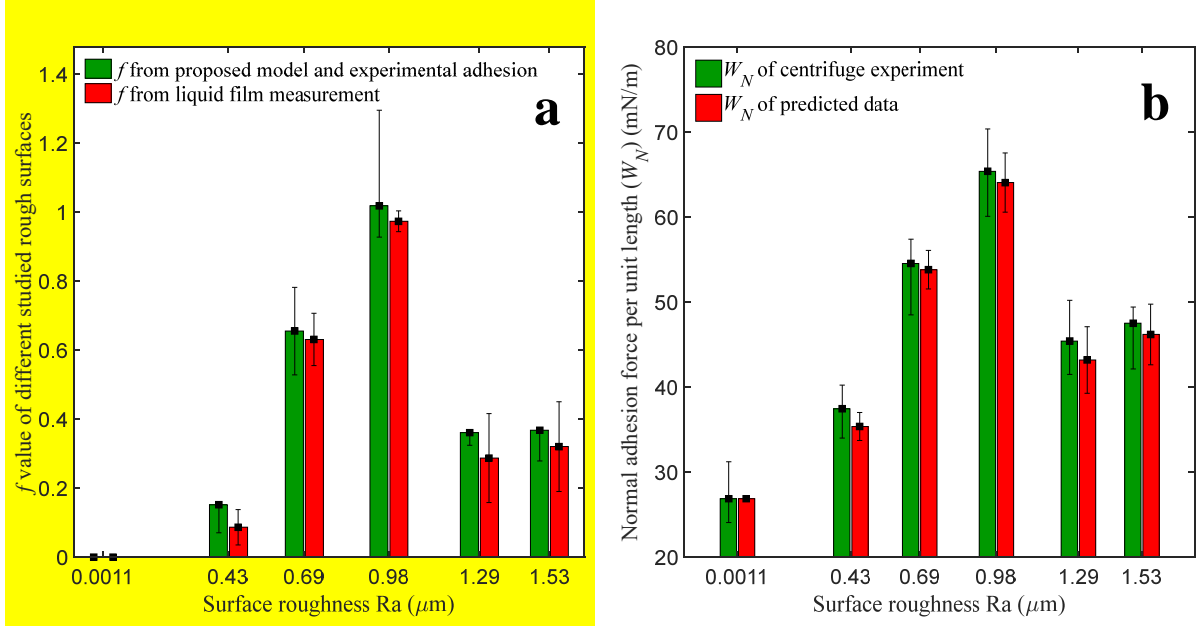
Fig. 9. (a) Comparison between measured f from remaining liquid film on the surface and that calculated from adhesion based on the proposed model. (b) Comparison between experimental W_N and predicted W_N based on the proposed model with measured f.

In order to find f, the liquid residue on different rough surfaces was observed by a microscope (Ni-E, Nikon, Japan). The detailed images of liquid film on each rough surface are shown in Fig. 8. We used the software ImageJ to measure the length of the liquid along the contact line so as to obtain the ratio f. The measuring method is detailed in Figure 3S and in the Supporting Information. The measured values of f are reported in Fig. 9a and the corresponding calculated work of adhesion are presented in Fig. 9b. The f value of the rough surface with Ra=0.98 μm is close to 1 and the liquid residue covers most of the rough surface including the grooves and small structures (Fig. 8d). It is also found that the work of adhesion (65.4 mN/m) in this case is close to the liquid surface tension (64.8 mN/m). For the smooth surface with Ra=0.0011 μm, almost no liquid residue is found on the surface and f is essentially zero. The calculated W_N by Equation (6) agrees well with

17

that from the centrifuge experiment except for some cases, they are a bit underestimated. It is because we can only measure the observable liquid-liquid contact line on the grooves under the microscope. However, there may be some liquid stuck in smaller microstructures, which is beyond the resolution of the microscope for observation. The absence of these liquids in measuring the effective ratio f would be the reason for the underestimation of W_N.

Fig. 9a shows that the f value first increases and then decreases quickly and remains almost constant, which determines and explains the W_N changing trend with surface roughness in this work. Since the liquid-liquid adhesion is larger than the solid-liquid adhesion in this experiment, for a larger f value, the contribution of liquid-liquid adhesion to overall adhesion is larger, thus, the overall adhesion is larger. However, the f value does not always increase with roughness. For the surfaces with larger roughness of Ra = 1.29 μm and 1.53 μm, the f value is smaller than that of the surface with Ra = 0.98 μm. From Fig. 8, it is seen that the f value depends on the surface morphology for a specific solid-liquid system. It is observed that most of the liquid attaches to the grooves with specific size (Fig. 8c and d); while liquid does not attach to the smaller or larger grooves (Fig. 8b, e, and f). For the liquid attachment in the surface grooves, there should be a capillary force balance among the solid-liquid interaction, liquid-liquid interaction with bulk liquid of droplet, and centrifugal force. Since in this study, we only quantified roughness by using Ra, further investigations on how detailed surface morphology affects f are recommended.

4.2. Comparison between experimental work of adhesion and estimations from Young-Dupré equation and Schrader's model

18

Tadmor et al. (Tadmor et al. 2017) proposed that the normal adhesion force per unit length. W_N, by this centrifuge method can be regarded as the work of adhesion (WA). Thus, the W_N is also compared with the WA calculated by some theoretical methods. The WA can be analysed from an energy perspective by the Young-Dupré equation (Dupré and Dupré 1869) or Schrader's model (Schrader 1995), which defines the WA as the energy difference per unit area before and after the droplet separation from a solid surface. The former assumes a droplet retains its original spherical cap after separation, but the latter assumes it forms a volume-equivalent spherical shape. However, the original approaches of these two models assume there is no liquid residue left on the solid surface after droplet detachment, which is only true for the case of a smooth surface. For the hydrophilic rough surfaces in this work, there are liquid films left on the rough surfaces contributing to the adhesion. Thus, we modify the Young-Dupré equation and Schrader's model by integrating the liquid film into the energy difference to calculate the WA. The detailed calculation process is shown in Figure 4S in the Supporting Information. The comparison of the current experimental results and the theoretical results is shown in Fig. 10.
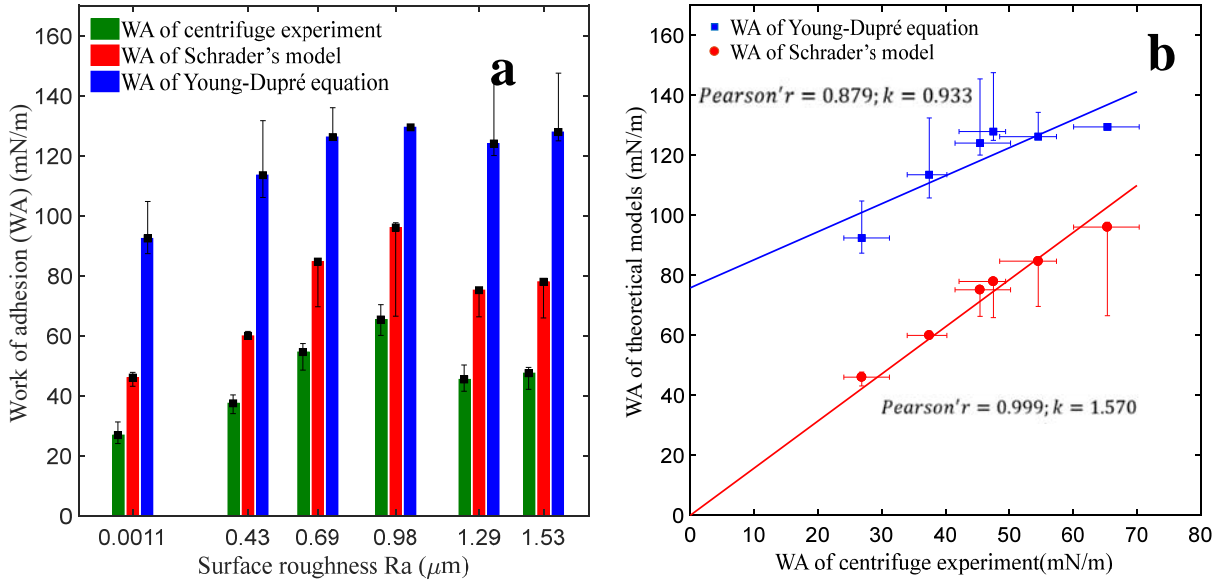
Fig. 10. Comparison of work of adhesion of centrifuge experiment, Young-Dupré equation, and Schrader's model. The vertical whiskers represent the work of adhesion ranges based on the receding and advancing contact angle. *Pearson'r* is the Pearson correlation coefficient, which indicates the strength of the linear relationship between paired data. *k* is the slope of the linear line.

Fig. 10a shows that the calculated values of the WA from the Young-Dupré equation and Schrader's model are larger than the experimental results, but the trends with surface roughness are identical. Fig. 10b shows that results of the two theoretical models have a positive linear relationship with the experimental data, which means the two models can well capture the effect of the liquid film on WA. The comparison of the three WAs is similar to the quantitative comparison in the references (Kuna et al. 2009, Voïtchovsky et al. 2010), in which the Young-Dupré equation results are larger than the AFM results but they have a positive linear relationship with each other. The quantitative comparison in Fig. 10 indicates that the WA from Schrader's model is closer to the experimental results than that from the Young-Dupré equation. It shows that the final sphere droplet after detachment assumed by the Schrader's model is much closer to the actual droplet separation mechanism under normal force. The following two reasons are the possible explanations for the overprediction. In the theoretical models, we did not consider the liquid volume loss on the surface due to capillarity action of the roughness, which would enlarge the volume of the final droplet compared with the actual case, and so the surface energy of the final sphere and WA would be overpredicted. In addition, the difference between the measured macroscale contact angle and the nanoscale contact angle is also an uncertainty that can cause the quantitative difference (Heepe et al. 2013, Tadmor et al. 2017).

4.3. Comparison between the W_N and W_L

It is found that W_N is much larger than W_L for each roughness even though the changing trends with roughness are similar. Moreover, the remaining liquid residues on rough surfaces under lateral detachment, as shown in Fig. 11, is much less than that under normal force, as shown in Fig. 8. The ratios of W_N to W_L are listed in Table 1. They range from 3.12 to 3.81 with mean value of 3.35±0.25 for different surface roughness. We also re-processed the data in Fu et al. (2018), which studied the microdroplet detachment on different substrate materials. The ratios of normal adhesion to lateral adhesion for smooth stainless steel (Ra = 3.13 nm), glass (Ra = 1.5 nm), and PMMA (Ra = 0.89nm) substrates are 3.487, 3.018, and 3.966 respectively. It indicates that the detachment mechanisms for a droplet under different applied force direction are different, but resulting in a similar ratio of W_N to W_L for different surface roughness and materials.

Table 1

Ratio of W_N to W_L

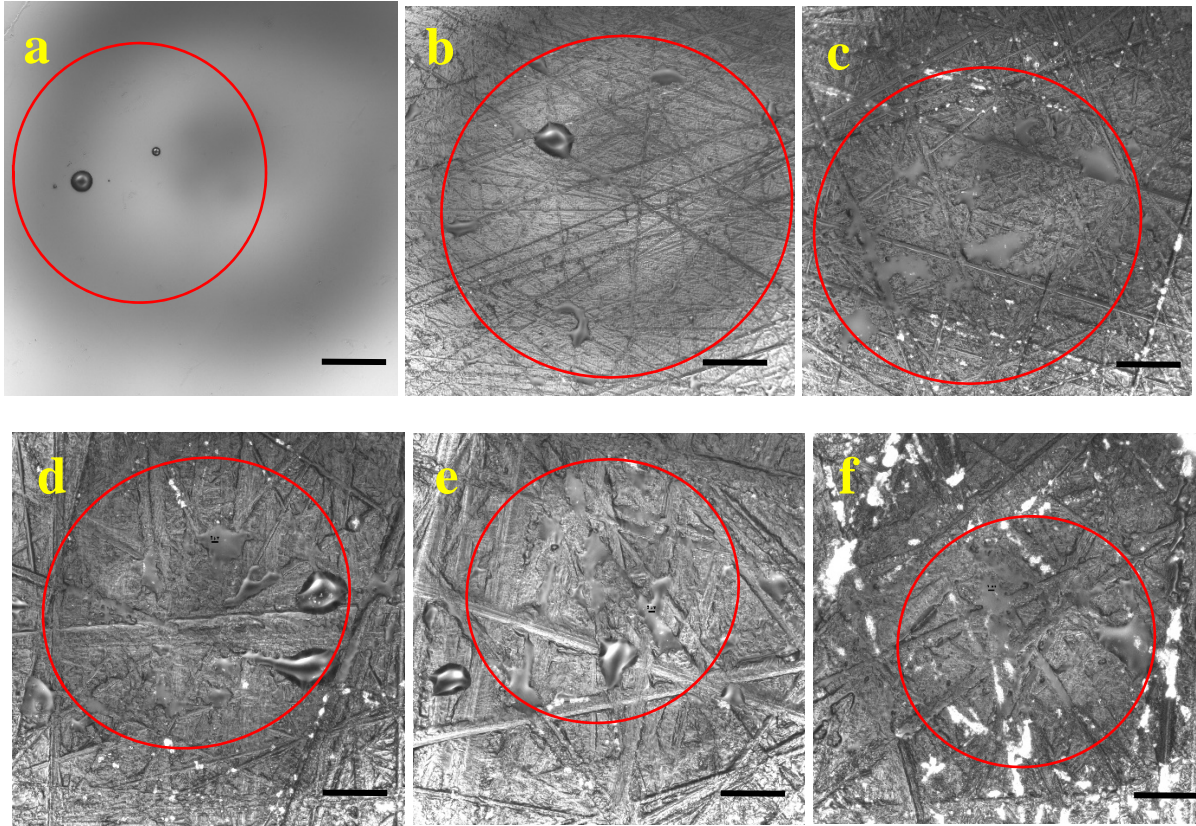| Ra (μm)	0.0011	0.43	0.69	0.98	1.29	1.53	Mean
W_N/W_L	3.81	3.45	3.12	3.31	3.20	3.22	3.35±0.25

Fig. 11. Detailed liquid film around the microdroplet after partial detachment under lateral force for all surfaces. Red circles indicate the original positions of the droplets before detachment. (a)-(f) are the surfaces with roughness: 0.0011, 0.43, 0.69, 0.98, 1.29, and 1.53 μm respectively. The scale bars in a-f are 50 μm.

## 4.4. Effect of surrounding liquid film on the further detachment behavior

It is observed that for the rough surfaces, some liquid films remain on the surface after droplet detachment. But there is no liquid film left on a smooth surface (Ra=0.0011 μm) as shown in Fig. 4 and Fig. 8a. Previously, we only focused on the detachment of droplets without liquid films surrounding. However, the existence of the initial liquid film around a droplet may subsequently

affect the droplet detachment. Thus, how the surrounding liquid film affects the further separation behavior is then studied.

Droplets surrounded by liquid films were prepared by droplet partial detachment under a specific normal force. The contact angle of the remaining droplet was measured again. The new contact angle (32.3°) of a droplet surrounded by a liquid film was found to be smaller than that without the surrounding liquid film (38.1°). Normal force and lateral force were exerted on the droplets again respectively. For normal detachment, the droplets still partially detached and became smaller, identical to those without the initial surrounding liquid film. However, for the lateral detachment, the behavior was different. Droplets were initially at the middle or edge of the liquid films. Under a moderate lateral force, droplets first moved to the edge of the circular liquid film, downstream of the force. When the lateral force was increased further, the droplet moved out of the liquid film and detached. The detachment processes under normal and lateral forces are shown in Fig. 12.
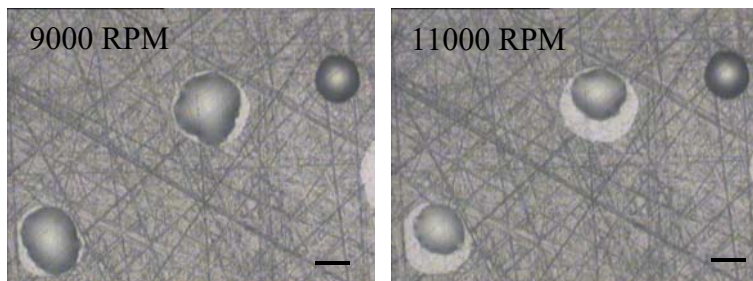
(a) Normal force
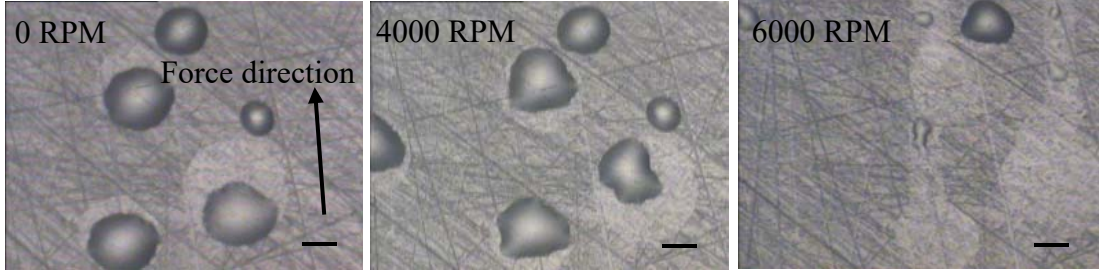
(b) Lateral force

Fig. 12. Droplet detachment behavior with surrounding liquid film under (a) normal force and (b) lateral force. The scale bars are 100 µm.
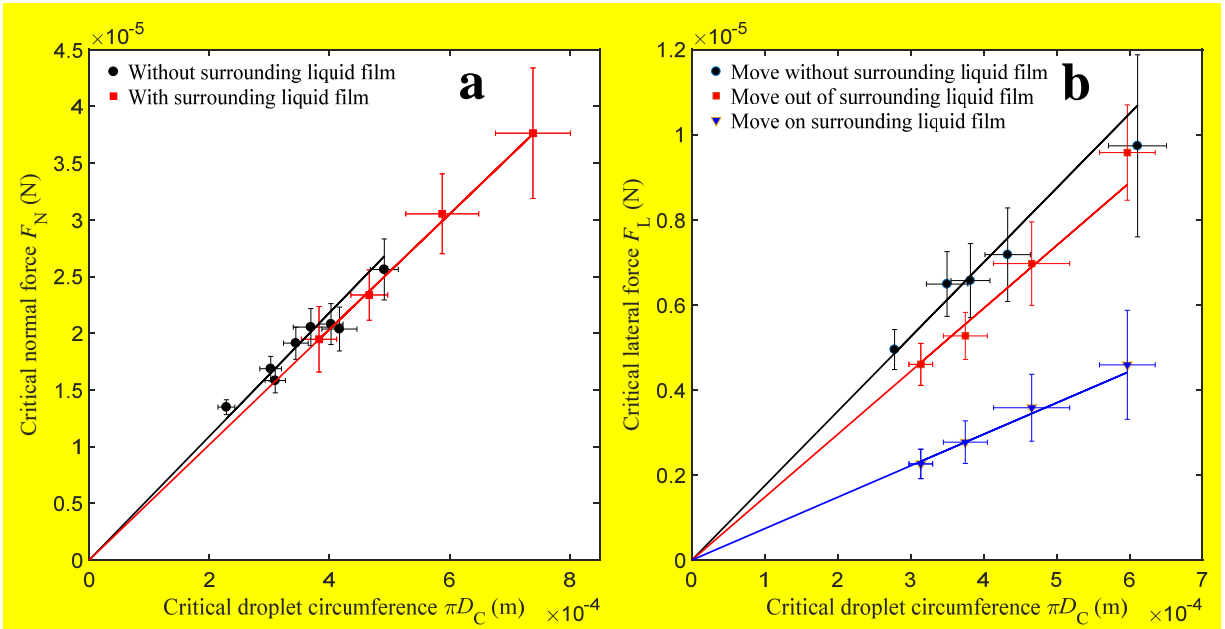

Fig. 13. Plots of normal force (a) and lateral force (b) against droplet circumference. The vertical and horizontal error bars in (a) are the differences of the forces and circumferences before and after detachment, respectively; the vertical and horizontal error bars in (b) are the two successively applied lateral forces and the standard deviation of detached microdroplet sizes, respectively.

As shown in Fig. 13a, the slopes of the linear lines which are the W_N for the cases with and without surrounding liquid film, are similar. It shows that the initial surrounding liquid film does

not change the W_N. However, the surrounding liquid film can significantly reduce the W_L. According to the droplet moving processes under lateral force, the droplet would move on the liquid film until the edge and then move out of the liquid film. Thus, two kinds of W_L were measured based on these two critical forces: critical force to start moving and critical force to move out of the liquid film (Fig. 13b). The ratio of the three W_L is *1.00/0.85/0.42* (without liquid film/moving out of liquid film/moving on liquid film). The W_L without initial liquid film is the largest, where the lateral force is used to overcome the pinning force of the solid-liquid three-phase contact line. When there exists an initial liquid film, the W_L becomes smaller, where the resistance is from the pinning force of the liquid film-liquid three-phase contact line. Since the initial contact surfaces and their area are identical for all three cases, the resistance at the separation process should be determined by the contact line, which agrees well with the fact that it is the contact lines, not the contact areas, which are important in determining wettability (Gao and McCarthy 2007). By comparing the case of move on surrounding film in Fig. 13b and the case of lateral detachment from the smooth surface in Fig. 5c, it is seen that the slopes (i.e. W_L) of these two cases are very similar. The reason behind is not clear and further investigation is recommended in the future.

5. Conclusions

In this work, we study the detachment behavior of a droplet from a rough hydrophilic surface under normal and lateral force by centrifuge. The normal adhesion force per unit length (W_N) is found to be related to the liquid film stuck in the surface microstructures. A new model, verified by the experiment, is proposed to consider the effect of the liquid film; W_N is a linear combination of liquid-liquid adhesion and solid-liquid adhesion. We then compare our model with the Young-Dupré equation and the Schrader's model and the changing trends are the same. We find that

25

adhesion is also subject to the removal force direction: the normal adhesion force per unit length (W_N) is about 3.35±0.25 times of lateral adhesion force per unit length (W_L) for the same surface. The study of the effect of an initial surrounding liquid film on droplet detachment shows that a surrounding liquid film does not affect the W_N for further separation but can reduce the W_L. The results in this work shed new understanding on the droplet resuspension from rough solid surfaces and can be used to predict the adhesion based on surface structure.

Declarations of interest

None.

Acknowledgments

References

Adamson, A. W., & Gast, A. P. (1967). Physical chemistry of surfaces, 6th edition.

Bergeron, V., Bonn, D., Martin, J. Y., & Vovelle, L. (2000). Controlling droplet deposition with polymer additives. *Nature*, 405(6788), 772.

Boreyko, J. B., & Chen, C. (2009). Restoring superhydrophobicity of lotus leaves with vibration-induced dewetting. *Physical Review Letters*, 103(17), 174502.

Cassie, A., & Baxter, S. (1944). Wettability of porous surfaces. *Transactions of the Faraday society*, 40, 546-551.

Dupré, A., & Dupré, P. (1869). *Théorie mécanique de la chaleur*: Gauthier-Villars.

Dussan, E. B. (1985). On the ability of drops or bubbles to stick to non-horizontal surfaces of solids. Part 2. Small drops or bubbles having contact angles of arbitrary size. *Journal of Fluid Mechanics*, 151(1).

Extrand, C. W., & Gent, A. N. (1990). Retention of liquid drops by solid surfaces. *Journal of colloid and interface science*, 138(2), 431-442.

Flick, E. W. (1998). 7.195 Viscosity of Aqueous Glycerol Solutions Centipoises. . In Anonymous *Industrial Solvents Handbook (5th Edition)*: William Andrew Publishing/Noyes.

Fu, S. C., Cheung, Y. S., Lee, H. H., Kwan, J. K., & Chao, C. Y. (2018). Studies on detachment behavior of micron sized droplets: A comparison between pure fluid and nanofluid. *Aerosol Science and Technology*, 52(1), 69-77.

Fu, S. C., Leung, W. T., & Chao, C. Y. (2014). Detachment of Droplets in a Fully Developed Turbulent Channel Flow. *Aerosol Science and Technology*, 48(9), 916-923.

Gao, L., & McCarthy, T. J. (2007). How Wenzel and Cassie were wrong. *Langmuir*, 23(7), 3762-3765.

Giorno, L., De Bartolo, L., & Drioli, E. (2003). Chapter 9 - Membrane bioreactors for biotechnology and medical applications. *Membrane Science and Technology*, 8, 187-217, doi: //doi.org/10.1016/S0927-5193(03)80012-8.

Gulec, S., Yadav, S., Das, R., & Tadmor, R. (2017). Reply to Comment on "Solid–Liquid Work of Adhesion". *Langmuir*, 33(48), 13899-13901.

He, B., Patankar, N. A., & Lee, J. (2003). Multiple equilibrium droplet shapes and design criterion for rough hydrophobic surfaces. *Langmuir*, 19(12), 4999-5003.

Heepe, L., Kovalev, A. E., Filippov, A. E., & Gorb, S. N. (2013). Adhesion failure at 180 000 frames per second: direct observation of the detachment process of a mushroom-shaped adhesive. *Physical Review Letters*, 111(10), 104301.

Hontanon, E., De los Reyes, A., & Capitão, J. A. (2000). The CAESAR code for aerosol resuspension in turbulent pipe flows. Assessment against the STORM experiments. *Journal of Aerosol Science*, 31(9), 1061-1076.

Jiang, J., Zhang, H., He, W., Li, T., Li, H., Liu, P., et al. (2017). Adhesion of Microdroplets on Water-Repellent Surfaces toward the Prevention of Surface Fouling and Pathogen Spreading by Respiratory Droplets. *ACS applied materials & interfaces*, 9(7), 6599-6608.

Kanematsu, H., & Yoshitake, M. (2015). Chapter 23 - Nanocomposite Coating for Antibacterial Purposes. *Handbook of Nanoceramic and Nanocomposite Coatings and Materials*, 489-513, doi: //doi.org/10.1016/B978-0-12-799947-0.00023-7.

Koishi, T., Yasuoka, K., Fujikawa, S., Ebisuzaki, T., & Zeng, X. C. (2009). Coexistence and transition between Cassie and Wenzel state on pillared hydrophobic surface. *Proceedings of the National Academy of Sciences*, 106(21), 8435-8440.

Kuna, J. J., Voïtchovsky, K., Singh, C., Jiang, H., Mwenifumbo, S., Ghorai, P. K., et al. (2009). The effect of nanometre-scale structure on interfacial energy. *Nature materials*, 8(10), 837.

Lafuma, A., & Quéré, D. (2003). Superhydrophobic states. *Nature materials*, 2(7), 457.

Lei, H., Li, Y., Xiao, S., Yang, X., Lin, C., Norris, S. L., et al. (2017). Logistic growth of a surface contamination network and its role in disease spread. *Scientific reports*, 7(1), 14826.

Leung, W. T., Fu, S. C., & Chao, C. Y. (2017). Detachment of droplets by air jet impingement. *Aerosol Science and Technology*, 51(4), 467-476.

Leung, W. T., Fu, S. C., Sze To, G. N., & Chao, C. (2013). Comparison of the resuspension behavior between liquid and solid aerosols. *Aerosol Science and Technology*, 47(11), 1239-1247.

Miwa, M., Nakajima, A., Fujishima, A., Hashimoto, K., & Watanabe, T. (2000). Effects of the surface roughness on sliding angles of water droplets on superhydrophobic surfaces. *Langmuir*, 16(13), 5754-5760.

Paxson, A. T., & Varanasi, K. K. (2013). Self-similarity of contact line depinning from textured surfaces. *Nature communications*, 4, 1492.

Prussin, A. J., & Marr, L. C. (2015). Sources of airborne microorganisms in the built environment. *Microbiome*, 3(1), 78.

Quéré, D. (2008). Wetting and roughness. *Annual Review of Materials Research*, 38, 71-99.

Rheinbaben, F. V., Schünemann, S., Gross, T., & Wolff, M. H. (2000). Transmission of viruses via contact in ahousehold setting: experiments using bacteriophage φX174 as a model virus. *Journal of Hospital Infection*, 46(1), 61-66.

Rusin, P., Maxwell, S., & Gerba, C. (2002). Comparative surface-to-hand and fingertip-to-mouth transfer efficiency of gram-positive bacteria, gram-negative bacteria, and phage. *Journal of applied microbiology*, 93(4), 585-592.

Schrader, M. E. (1995). Young-dupre revisited. *Langmuir*, 11(9), 3585-3589.

Tadmor, R., Das, R., Gulec, S., Liu, J., E. N'guessan, H., Shah, M., et al. (2017). Solid–liquid work of adhesion. *Langmuir*, 33(15), 3594-3600.

Tadmor, R. (2004). Line energy and the relation between advancing, receding, and young contact angles. *Langmuir*, 20(18), 7659-7664.

Voïtchovsky, K., Kuna, J. J., Contera, S. A., Tosatti, E., & Stellacci, F. (2010). Direct mapping of the solid–liquid adhesion energy with subnanometre resolution. *Nature Nanotechnology*, 5(6), 401.

Wenzel, R. N. (1949). Surface roughness and contact angle. *The Journal of physical chemistry*, 53(9), 1466-1467.

Wenzel, R. N. (1936). Resistance of solid surfaces to wetting by water. *Industrial & Engineering Chemistry*, 28(8), 988-994.

Wyman, P. (2012). Hydrophilic coatings for biomedical applications in and ex vivo. *Coatings for Biomedical Applications*, 3-42.

Xu, W., & Choi, C. (2012). From sticky to slippery droplets: dynamics of contact line depinning on superhydrophobic surfaces. *Physical Review Letters*, 109(2), 024504.

Yoshimitsu, Z., Nakajima, A., Watanabe, T., & Hashimoto, K. (2002). Effects of surface structure on the hydrophobicity and sliding behavior of water droplets. *Langmuir*, 18(15), 5818-5822.

Droplet detachment behavior from a rough hydrophilic surface

C. T. Wang[1], W. T. Leung[1], J. C. Xu[1], S. C. Fu[2], and Christopher Y. H. Chao[2]*

[1] Department of Mechanical and Aerospace Engineering, The Hong Kong University of Science

and Technology, Hong Kong, China

[2] Department of Mechanical Engineering, The University of Hong Kong, Hong Kong, China

[*]Corresponding author: *cyhchao@hku.hk*

Address all correspondence to:

Christopher Y. H. Chao

Dean of Engineering and Chair Professor of Mechanical Engineering
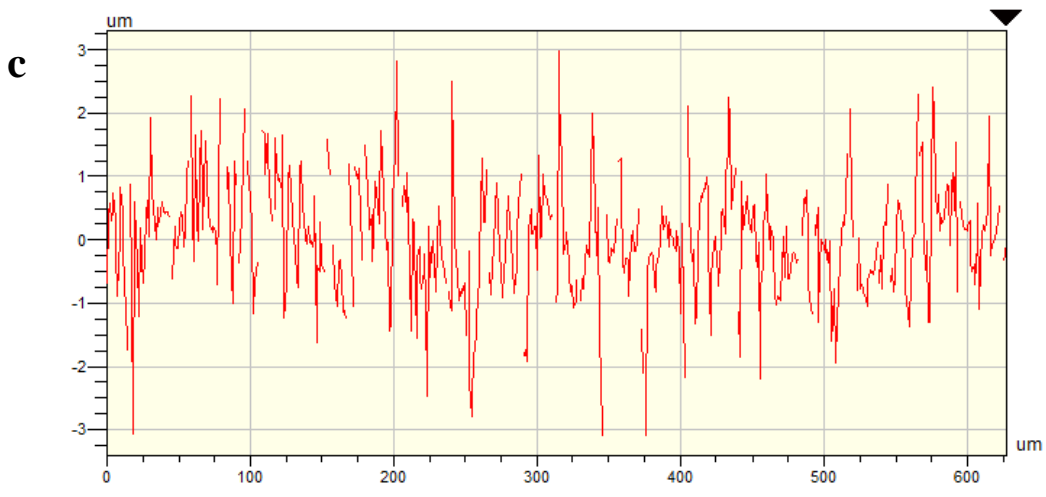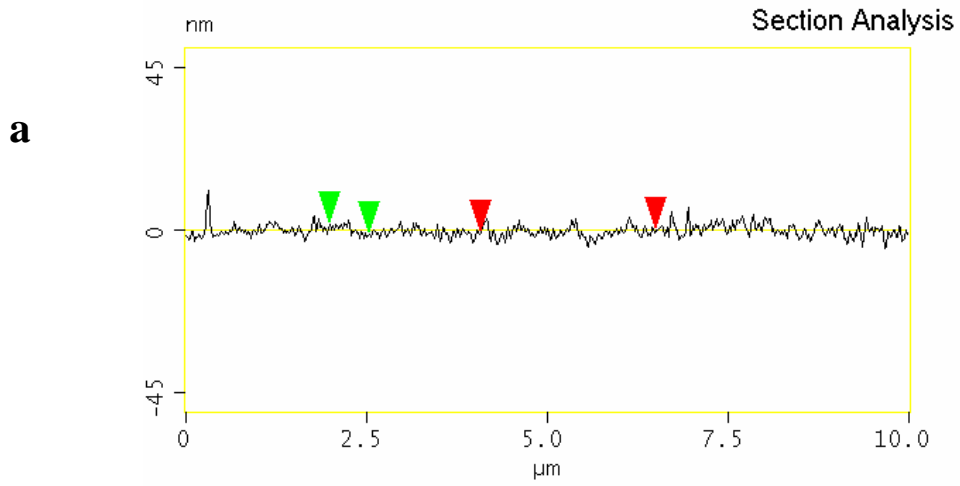
The University of Hong Kong

Pokfulam,

Hong Kong, China

Email: cyhchao@hku.hk
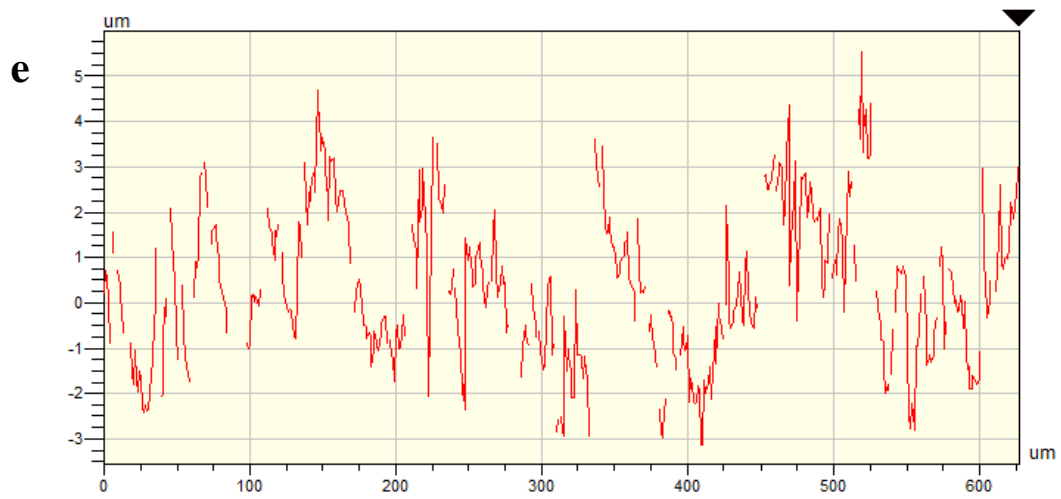
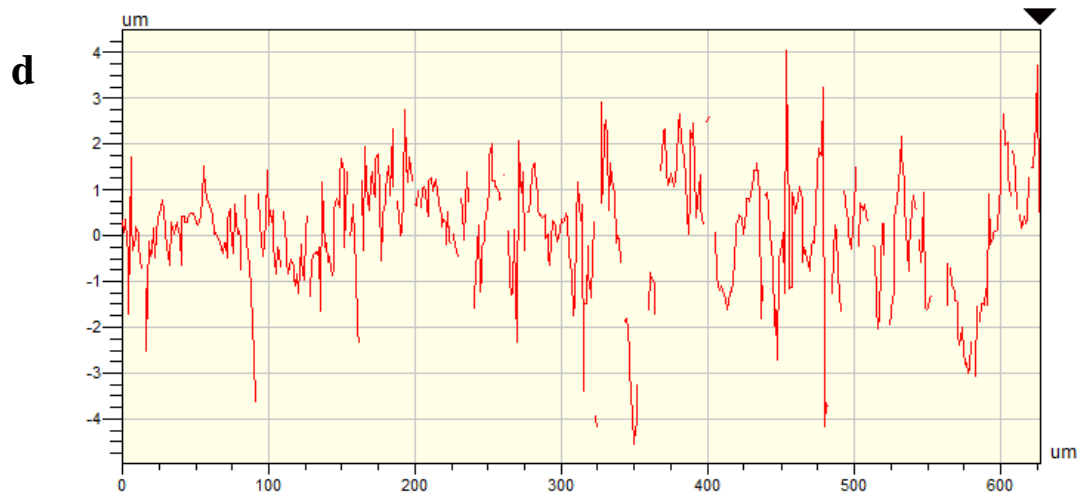Fax: (852) 2858-5415

Tel: (852) 3917-2800

d

e

f

Figure 1S. The surface profiles of the studied rough surfaces. (a) - (f) are the 2D surface profiles of Ra= 0.0011, 0.43, 0.69, 0.98, 1.29, and 1.53 µm respectively. <mark>(a) is from the atomic force microscope (AFM); (b) – (f) are from the optical profiler.</mark>
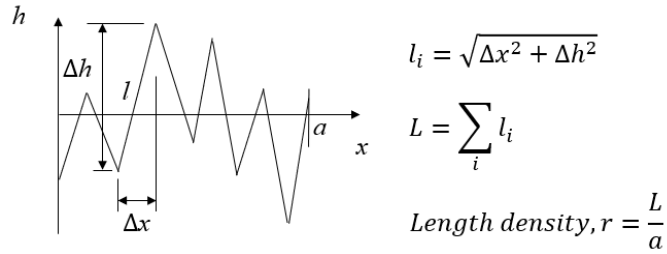
$$l_i = \sqrt{\Delta x^2 + \Delta h^2}$$

$$L = \sum_i l_i$$

$$Length\ density, r = \frac{L}{a}$$

Figure 2S. Schematic structure of sample and calculation of length density r

Table 1S.

The length density r of each studied surface

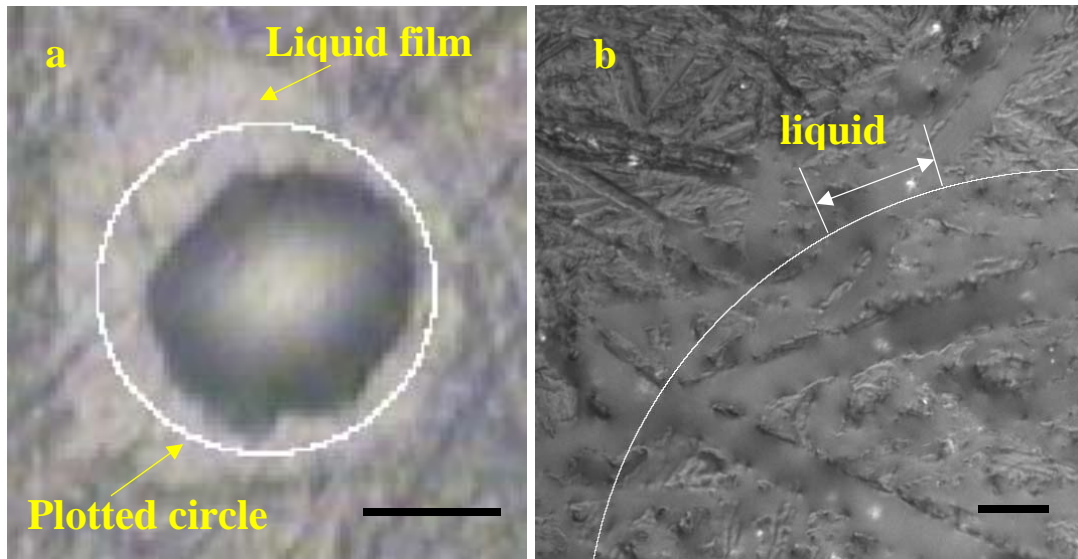| Ra (µm)	0.0011	0.43	0.69	0.98	1.29	1.53
r	1	1.212±0.048	1.301±0.069	1.319±0.074	1.283±0.059	1.392±0.080

Figure 3S. Schematic diagram of measuring f based on the detailed picture of liquid film. (a) is the overview of a droplet surrounded by a liquid film and the plotted circle of contact line around the droplet; (b) is the enlarged local liquid film. The scale bars in (a) and (b) are 50 µm and 10 µm, respectively.

Procedures for measuring f: We first plotted a circle inside the liquid film to represent the critical contact line in detachment process as shown in Fig. 3Sa. Because the liquid film is very similar to a thin circular ring due to the small difference between D_1 and D_2. For the rough surfaces in this work, we find that the f value is independent of the position of plotted circle inside the thin liquid films. Then we identified the line segments that covered by liquid as shown in Fig. 3Sb. After measuring the total length of the liquid segments, the value of f can be obtained by finding the ratio of the length of the liquid segments to the circle circumference. Finally, we can acquire the mean f value for this rough surface from many different droplets.
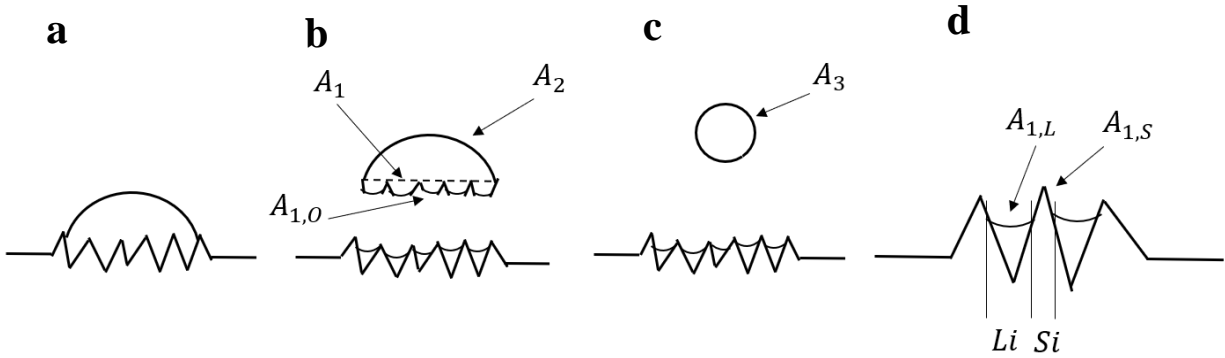
Figure 4S. Schematic diagram of calculating the work of adhesion by using the Young-Dupré equation and the Schrader's model by integrating the effect of liquid film. (a) is the initial state; (b) is the final state of the Young-Dupré equation; (c) is the final state of the Schrader's model; (d) is an enlarged schematic diagram of liquid film on the surface.

The created and disappeared surfaces before and after droplet separation are shown in the following items and denoted in Fig. 4S. The liquid line ratio f can also be interpreted as the area ratio because the plotted circle for f is crossing a thin circular ring. Thus, in the following we use the line ratio f as area ratio.

$$f = \frac{\sum Li}{\sum Li + Si} = \frac{\sum A_{1,L}}{\sum A_1}$$

Item 1: Created liquid surface of spherical cap base: $A_{1,O} = A_1 * ((1 - f) * r + f)$

Item 2: Created liquid surface on rough surface: $A_{1,L} = f * A_1$

Item 3: Created naked solid surface on rough surface: $A_{1,S} = A_1 * (1 - f) * r$; where r is length density measured from optical profiler shown in Fig. 1S.

Item 4: Disappeared solid-liquid interface: $A_{1,S}$

Item 5: Disappeared initial spherical liquid cap surface: A_2; calculated from A_1 and contact angle

Item 6: Created final sphere liquid surface: A_3; calculated from A_1 and contact angle (equivalent volume)

For the Young- Dupré equation (Dupré and Dupré 1869) , the energy difference contains the items 1, 2, 3, and 4. For Schrader's model (Schrader 1995) , the energy difference contains energy difference of the Young- Dupré equation and the items 1, 5, and 6. Thus, the work of adhesion integrating the liquid film can be written as the following equations.

Young-Dupré equation

$$E \; of \; Young - Dupré \; equation = \; A_{1,0} * \gamma_L + A_{1,L} * \gamma_L + A_{1,S} * \gamma_S - A_{1,S} * \gamma_{S,L}$$

$$W, Young - Dupré \; equation \; = \frac{E \; of \; Young - Dupré \; equation}{A_1}$$

Schrader's model

$$E \; of \; Schrader's \; model = E \; of \; Young - Dupré \; equation + \left(A_3 - A_2 - A_{1,0}\right) * \gamma_L$$

$$W, Schrader's \; model \; = \frac{E \; of \; Schrader's \; model}{A_1}$$

The solid-liquid interfacial energy of each studied surface is calculated by the following Young equation:

$$\gamma_{S,L} = \gamma_S - \gamma_L * cos\theta$$

where γ_S is solid surface energy, which is from the database (Krevelen†, D.W. van Nijenhuis, K. te. 2009); θ is equilibrium contact angle, which is measured from goniometer of droplet on the smooth surface.

References

Dupré, A., & Dupré, P. (1869). *Théorie mécanique de la chaleur*: Gauthier-Villars.

Krevelen†, D.W. van Nijenhuis, K. te. (2009). *Properties of Polymers - Their Correlation with Chemical Structure; Their Numerical Estimation and Prediction from Additive Group Contributions (4th, Completely Revised Edition) - 8.3.3 Numerical Values and Comparison of the Different Methods. Elsevier. Retrieved from https://app.knovel.com/hotlink/pdf/id:kt00984AW1/properties-polymers-their/numerical-values-comparison*.

Schrader, M. E. (1995). Young-dupre revisited. *Langmuir*, 11(9), 3585-3589.